Nanoparticle Targeted Folate Receptor 1-Enhanced Photodynamic Therapy for Lung Cancer

Tatsuya Kato[a,b]*, Cheng S. Jin[c,d,e]*, Hideki Ujiie[a], Daiyoon Lee[a], Kosuke Fujino[a], Hironobu Wada[a], Hsin-pei Hu[a], Robert A. Weersink[e], Juan Chen[f], Mitsuhito Kaji[g], Kichizo Kaga[b], Yoshiro Matsui[b], Brian C. Wilson[e,f], Gang Zheng[c,d,e,f,h], and Kazuhiro Yasufuku[a,d,e,h]**

[a]Division of Thoracic Surgery, Toronto General Hospital, University Health Network, Toronto, Canada

[b]Department of Cardiovascular and Thoracic Surgery, Hokkaido University Graduate School of Medicine, Sapporo, Japan

[c]Graduate Department of Pharmaceutical Sciences, Leslie Dan Faculty of Pharmacy, University of Toronto, Canada

[d]Institute of Biomaterial and Biomedical Engineering, University of Toronto, Canada

[e]Guided Therapeutics, Princess Margaret Cancer Centre and TECHNA Institute, University Health Network, Canada

[f]Department of Medical Biophysics, University of Toronto, Canada

[g]Department of Thoracic Surgery, Sapporo Minami-sanjo Hospital, Sapporo, Hokkaido, Japan

[h]Division of Experimental Therapeutics, Respiratory & Critical Care, Princess Margaret Cancer Centre, Canada

*co-first authors

**Correspondence should be addressed to:

Kazuhiro Yasufuku, MD, PhD

Director, Interventional Thoracic Surgery Program

Associate Professor, University of Toronto

Division of Thoracic Surgery, Toronto General Hospital, University Health Network

200 Elizabeth St, 9N-957, Toronto, ON M5G2C4, Canada

Phone: 416-340-4290, Fax: 416-340-3660

E-mail: kazuhiro.yasufuku@uhn.ca

Running title: Folate receptor targeted PDT in lung cancer

Keywords: photodynamic therapy (PDT); lung cancer; folate receptor 1 (FOLR1); porphysome;

ABSTRACT

Objective: Despite modest improvements, the prognosis of lung cancer patients has still remained poor and new treatment are urgently needed. Photodynamic therapy (PDT), the use of light-activated compounds (photosensitizers) is a treatment option but its use has been restricted to central airway lesions. Here, we report the use of novel porphyrin-lipid nanoparticles (porphysomes) targeted to folate receptor 1 (FOLR1) to enhance the efficacy and specificity of PDT that may translate into a minimally-invasive intervention for peripheral lung cancer and metastatic lymph nodes of advanced lung cancer.

Materials and methods: The frequency of FOLR1 expression in primary lung cancer and metastatic lymph nodes was first analyzed by human tissue samples from surgery and endobronchial ultrasonography-guided transbronchial needle aspiration (EBUS-TBNA). Confocal fluorescence microscopy was then used to confirm the cellular uptake and fluorescence activation in lung cancer cells, and the photocytotoxicity was evaluated using a cell viability assay. *In vivo* fluorescence activation and quantification of uptake were investigated in mouse lung orthotopic tumor models, followed by the evaluation of *in vivo* PDT efficacy.

Results: FOLR1 was highly expressed in metastatic lymph node samples from patients with advanced lung cancer and was mainly expressed in lung adenocarcinomas in primary lung cancer. Expression of FOLR1 in lung cancer cell lines corresponded with the intracellular uptake of folate-porphysomes *in vitro*. When irradiated with a 671 nm laser at a dose of 10 J/cm^2, folate-porphysomes showed marked therapeutic efficacy compared with untargeted porphysomes (28% *vs.* 83% and 24% *vs.* 99% cell viability in A549 and SBC5 lung cancer cells, respectively). Systemically-administered folate-porphysomes accumulated in lung tumors

with significantly enhanced disease-to-normal tissue contrast. Folate-porphysomes mediated PDT successfully inhibited tumor cell proliferation and activated tumor cell apoptosis.

Conclusion: Folate-porphysome based PDT shows promise in selectively ablating lung cancer based on FOLR1 expression in these preclinical models.

(299/ 300 words)

1. Introduction

Lung cancer is the leading cause of cancer-related mortality worldwide (1). Currently, more lung cancer patients are being diagnosed at an earlier stage due to improved diagnostic imaging (2). Although surgical resection has always been considered the standard treatment for patients with early-stage NSCLC, some patients are excluded due to significant co-morbidities (3). Hence non-surgical treatment options have evolved significantly over the past decade, including stereotactic body radiotherapy (SBRT) and radiofrequency ablation (RFA). However, SBRT has imperfect local-regional control and cannot be used for local recurrent disease included in the primary radiation field (4). Percutaneous RFA has low accessibility to many cancers and is inferior in outcome to surgery (5). Photodynamic therapy, PDT, has been performed as an alternative treatment in lung cancer (6-8). Successful PDT ablation with minimal invasiveness is highly dependent on precise light delivery and tumor-specific accumulation of photosensitizers. However, access for light delivery is restricted by the location of the tumor, which limits the treatment to carcinoma *in-situ* and palliation of the advanced obstructing lung cancer in the central airway (9, 10). Technical advances in minimally-invasive PDT treatment promise a shift towards using PDT as first treatment choice for early-stage lung cancer.

Radial probe endobronchial ultrasound (EBUS) has been considered a useful technique in addition to conventional bronchoscopy to improve the efficacy of PDT in patients with centrally-located early-stage lung cancer (6, 11). We have previously integrated an ultra-thin optical fiber into TBNA needle and demonstrated transbronchial PDT under navigation bronchoscopy (12, 13). Besides the precise light delivery, tumor targeting of the PDT photosensitizer adds specificity to the treatment. Different strategies have been explored for

this purpose to achieve tumor-preferential accumulation of photosensitizer and the tumor-specific activatable photosensitizers. For the latter, after initial accumulation in the tumor the photosensitizers are ‘photodynamically inactive’ due to photophysical suppression (quenching) of the cytotoxic singlet-oxygen generation. However photoactivity is regained through mechanisms such as enzymatic-, nucleic acid- (14, 15) or microenvironmental activation (pH, hydrophobicity, etc.) (16, 17). This enables a degree of selectivity to kill only the target cancer cells.

In this study, we introduce an activatable photosensitizer for tumor-specific PDT, named folate receptor-targeted porphysomes. Porphysomes are all-organic bilayer liposome-like nanoparticles that self-assemble from porphyrin-lipid conjugates. They have intrinsic multimodal capabilities for both imaging and therapy (18, 19). Because of the extremely high porphyrin packing density (>80,000 per particle) in the phospholipid bilayer, both fluorescence and singlet oxygen generation are highly quenched (>99%) in intact porphyrins (19) but these are restored once the nanoparticles are internalized into the cancer cells. Recently, based on the finding that folate receptor 1 (FOLR1) is overexpressed in various cancers (20), we have integrated folic acid into the nanostructure to generate ‘folate-porphysomes’ (FP) to enhance tumor targeting that also re-activates the PDT efficacy (20). Hence, FP-PDT has emerged as a promising new strategy to treat lung cancers with over-expression of FOLR1. Based on these findings, the aim of the present study is to evaluate FPs in preclinical lung cancer models as a potential minimally-invasive treatment for lung cancer.

We firstly examined the expression of FOLR1 on multiple lung cancer cell lines, and evaluated the specificity of FPs in targeting cell lines with overexpressed FOLR1. The therapeutic efficacy of FP-PDT was then evaluated both *in vitro* using lung cancer cell lines

and *in vivo* on the mice bearing subcutaneous lung tumors. Finally, the specificity of FP-PDT was evaluated in A549 lung tumors grown orthotopically in mice. The quantitative biodistribution of FPs was also analyzed in the orthotopic model to assess the potential of future translational studies in treating peripheral lung cancer.

2. Materials and methods

2.1. Lung cancer tissue samples and cell lines

Seventeen samples taken from metastatic lymph nodes from lung cancers were obtained via EBUS-TBNA from patients at Toronto General Hospital and a total of 333 NSCLC samples for tissue microarray (TMA) were obtained at Hokkaido University and affiliated hospitals with informed consents (21-23) (**Table 1**). Histological diagnosis was based on the WHO Classification (4^{th} Ed.) (24). All tumors were staged according to the pathological TNM classification of the International Union against Cancer (7^{th} edition) (25). All specimens were fixed in formalin and embedded in paraffin wax. Representative blocks were selected (based primarily on greatest dimensions of each tumor), and serial 4 μm-thick sections were examined by immunohistochemistry. Histological diagnosis was based on the World Health Organization Classification (4^{th} Ed.) (24). All tumors were staged according to the pathological tumor/node/metastasis (pTNM) classification of the International Union against Cancer (7^{th} edition) (25).

A series of human lung cancer cell lines were used: ADC DFC1024, DFC1032, NCI-H2228, NCI-H1975, NCI-H3255, NCI-H4006, NCI-H1650, NCI-H1819, NCI-H2009, NCI-H2030, NCI-H2122, NCI-H2405, NCI-H1437, A549, HCC827, HCC2279, HCC2935, HCC4011, and

HCC4019; lung ASC NCI-H647; lung SqCC MGH7; lung large cell carcinoma (LCC) NCI-H460, H460SM, and NCI-H661. SCLC SBC-5, EBUS-060 and KB cells were kindly provided by Dr. Ming-Sound Tsao (UHN, Toronto). Cells were grown in monolayers in appropriate medium supplemented with 10% FCS and maintained at 37°C in humidified air with 5% CO_2.

2.2. Quantitative reverse transcription-polymerase chain reaction (qRT-PCR)

cDNA was synthesized from 2 µg total RNA using a QuantiTect® Reverse Transcription Kit (Qiagen). The primers were designed as follows: for FOLR1, forward primer, 5'-aagtgcgcagtgggagct-3', and reverse primer 5'- cattgcacagaacagtgggtg-3'; for actin, beta (ACTB), forward primer, 5'-gaaatcgtgcgtgacattaa-3', and reverse primer, 5'-aaggaaggctggaagagtg-3'. qRT-PCR analysis was performed using LightCycler480® SYBR Green I Master Ready-to-use hot start reaction mix and LightCycler480® system (Roche, South San Francisco, CA, USA). The thermal cycler conditions were 5 min at 95.0 °C for denaturation, 45 cycles at 95°C for 10 s, 56°C for 10 s, 72°C for 10 s for PCR amplification and 1 min at 65°C for melting. The threshold cycle value was defined as the value when the fluorescence signal increased above the background threshold. PCR reactions were carried out in triplicates.

2.3. FOLR1 immunohistochemistry

FOLR1 immunostaining was performed using an automated IHC platform (Autostainer Plus, DAKO Corp., Carpinteria, CA, USA). Anti-FRA monoclonal antibody (Novocastra™ Liquid Mouse Monoclonal Antibody, Folate Receptor Alpha, Leica, Newcastle, UK) was

diluted 30-fold using mixed antibody diluent (DAKO: S2022 Antibody Diluent). After incubation with the primary antibody at 4°C overnight, a polymer-based detection system (EnVision™+ Dual Link #K4063, DAKO) was used with 3', 3-Diaminobenzidine (DAB) as the chromogen. Positive controls included a sample of kidney, while normal lung samples were used as negative controls. Slides were dehydrated and placed on coverslips.

2.4. Western Blotting

After cells were grown to >80% confluency, they were lysed using RIPA buffer (pH 7.5, 50 mmol/L Tris-HCl, 1 mmol/L EDTA, 100 mmol/L NaCl, 1% Triton X-100) containing protease inhibitors (20 µmol/L leupeptin, 0.8 µmol/L aprotinin, 10 µmol/L pepstatin and 1.25 mmol/L phenylmethylsulfonyl fluoride). Lysates were incubated for 15 min on ice and centrifuged at 14,000 rpm for 10 min at 4°C. Total protein in the supernatant was quantified using a BCA protein assay reagent kit (Bio-Rad, Mississauga, ON, Canada). Equal amount of protein were loaded for each cell line onto a 10% SDS-PAGE gel and run at 100 V for 90 min. Proteins were then transferred onto a nitrocellulose membrane using a Miniprotein III electro-blotter (Bio-Rad, Mississauga, ON, Canada). These immunoblots were washed in TBS containing 0.1% Tween-20 and probed overnight at 4°C with primary antibody (Anti-Folate Binding Protein antibody [EPR4708(2)], ab125030, 1/1,000 dilution Abcam, UK). Membranes were washed and incubated for 1 h with secondary antibody at room temperature. Bound antibodies were then detected using a film developer after treatment with commercial Super Signal containing enhanced luminol and oxidizing agents (ECL, Amersham Pharmacia Biotech, Freiburg, Germany).

2.5. Porphysome synthesis

Regular (i.e. non-targeted) porphysomes and FPs were synthesized following a protocol reported previously (18). Briefly, the lipid film for regular porphysomes consisted of 55 mol% of porphyrin-lipid (pyropheophorbide-lipid), 40 mol% of cholesterol (Avanti Polar Lipids), and 5 mol% of distearoyl-sn-glycero-3-phosphoethanolamine-N-methoxy(polyetheneglycol) (PEG2000-DSPE; Avanti Polar Lipids, USA) (20). For FPs 1 mol% 1,2-distearoyl-sn-glycero-3-phosphoethanolamine-N folate (polyethylene glycol) (Folate-PEG2000-DSPE; Avanti) was added to the 4 mol% PEG2000-DSPE(20). The resulting 10 mg lipid film was dried using a gentle stream of nitrogen gas and the remaining solvent was removed with 1 h vacuum. The dried lipids were stored at -20 °C in argon until porphysome synthesis. In order to make the porphysomes, 2.0 mL PBS buffer (150×10^{-3} M, pH 7.5) was added to the lipid film and the solution underwent 5 cycles of freeze-and-thaw to produce the lipid suspension of 5 mg/mL. It was then extruded through a polycarbonate membrane (100 nm pore size) 10 times under high pressure to form the nanoparticles of around 100 nm diameter, as measured by dynamic light scattering (ZS90 Nanosizer, Malvern Instruments) and the porphyrin concentration was determined by UV–Vis spectrometry (Varian Inc., Palo Alto, CA). All regular porphysomes and folate-porphysomes were prepared fresh for each experiment and kept sterile at 4°C.

2.6. Confocal microscopy and in vitro PDT

The fluorescence of intact porphysomes is highly quenched, but the nanostructure dis-assembles and the fluorescence is reactivated upon internalization into cells (18, 20). To validate the folate receptor targeting of FPs the cellular update was firstly compared the various lung cancer cell lines, based on fluorescence confocal microscopy. All images in

Figure 2A were made under the same conditions. FOLR1-positive A549, H647, H460 and SBC5 were used as the positive cell lines, while FOLR1-negative DFC1024 cell was the negative control. In addition, free folic acid was used as an inhibitor to further confirm the folate-receptor mediated internalization. For each cell line, 1 x 10^5 cells were seeded in a 2-well chamber slide (Lab-Tek™, Sigma-Aldrich, Oakville, Canada) and incubated for 24 h at 37 °C. The medium was then removed and replaced with three different treatment media containing either non-targeted porphysomes (5 x 10^{-6} M), FPs (5 x 10^{-6} M) or FPs (5 x 10^{-6} M) with free folic acid (1 x 10^{-3} M) for 3 h at 37°C. The cells were then rinsed with PBS 3 times and allowed to grow for 21 h in regular culture medium at 37 °C. 4% paraformaldehyde was used to fix the cells. Fluorescent mounting medium (Dako, Glostrup, Denmark) was used to prolong the fluorescent signal. A laser scanning confocal microscopy (FV 1000, Olympus, Tokyo, Japan) with excitation wavelengths of 405 and 633 nm were used to visualize DAPI and porphysome fluorescence, porphyrins, respectively.

Once the FPs internalize the PDT activity of the constituent porphyrins is also restored (20). To verify the activatable photocytotoxicity of the FPs, *in vitro* PDT and dark cytotoxicity were measured. A549 and SBC5 cells were seeded at a concentration of 5 x 10^3 cells/well in 96-well black walled plates (#655946, CELLCOAT®, Greiner Bio-One, Germany) 24 h prior to porphysome incubation. The cells were then treated with non-targeted (5 x 10^{-6} M) porphysomes, FPs (5 x 10^{-6} M) or FPs (5 x 10^{-6} M) with free folic acid (1 x 10^{-3} M) for 3 h at 37 °C, washed 3 times with PBS and incubated for 21 h in fresh medium. PDT was given using a 671 nm CW diode laser at light dose of 5 or 10 J/cm^2 at 100 mW/cm^2. The incubation medium was replaced with normal medium, and a proliferation assay (CellTiter96® AQueous One Solution Cell Proliferation Assay, Promega, Madison, WI, USA) was performed 24 h later

according to the manufacturer's instructions. Each experiment was performed in quadruplicate. Absorbance at 630 nm was measured using a μQuant microplate reader (Bio-Tek Instrument Inc., Winooski, VT, USA), with the absorbance at 490 nm serving as the background, to determine the relative viability compared to untreated controls. Replicate plates using the same materials, concentrations and incubation time but without the laser irradiation were used to assess the dark toxicities.

2.7. Mouse subcutaneous and orthotopic lung cancer models

All animal studies were conducted with instructional Animal Care Committee approval (AUP4151 and AUP 4449, University Health Network). Female nude mice were used for the *in vivo* subcutaneous and lung orthotopic lung cancer models. For the former 1 $x10^6$ cells in a 100 μL volume of Matrigel® was injected into the right thigh. The tumor size was monitored once every 2 days by calipers. The orthotopic model was as described previously (26). Briefly, the animal was positioned supine recumbent with the head elevated 90^o using a rubber band attached to the front upper teeth. Pulling the tongue laterally using a Mosquito-pean forceps raised the lower jaw and exposed the glottis. Under direct visualization of the vocal cords using a surgical microscope with x10 magnification, a 23-gauge 2.5-cm blunt-tip slightly curved metal catheter (Harvard Apparatus, Holliston, MA, USA) was introduced into the trachea. 70 μL tumor cell suspension (1.0×10^6 cells) was mixed with Matrigel® and administered into the lung. Tumor growth was monitored biweekly micro-CT scans. The mice were also monitored frequently for abnormal physiological changes (activities, body weight, etc.) and we consider any abnormal observation was used as the humane endpoint.

2.8. Accumulation of folate-porphysomes in subcutaneous tumor model

The accumulation of FPs in the subcutaneous FOLR1+ A549 and H460 tumors was determined following tail vein injection of 10 mg/kg (total lipid) of regular porphysomes or FPs. At 6 h post-injection the tumor fluorescence was imaged using a whole-mouse system (Maestro® EX 2.10, Cambridge Research & Instrumentation, Inc., Waltham, MA, USA) with 575-605 nm excitation and >645 nm detection using 500 ms integration time (n=4).

2.9. In vivo photodynamic Therapy

After confirming the tumor-preferential accumulation of FPs the *in vivo* PDT efficacy was evaluated as follows. The mice were subcutaneously inoculated with A549 cells (FOLR1-positive) as above (20) and allowed to grow to 5-6 mm diameter. Under general anesthesia (1.0 L/min O_2 and 2% isoflurane, followed by intraperitoneal injection of a xylazine/ketamine cocktail at 0.1 ml/10g body weight (xylazine 20 mg/ml, ketamine 100 mg/ml). At 6 or 24 h post porphysome injection, PDT was performed with a 671 nm diode laser (DPSS LaserGlow Technologies, Toronto, Canada) using a 10 mm spot diameter, 100 mW/cm^2 for a light dose at 100 J/cm^2.

The tumor size was then measured by calipers 3 times per week and the volume was calculated as V = (long radius)(short radius)^2/2 to provide the means and standard errors in each treatment group. The mice were euthanized by CO_2 treatment followed by head-and-neck dislocation at a defined end point when the short radius reached 15 mm. Tumors were harvested and fixed in 10% formaldehyde for 24 h prior to H&E and Ki67 and cleaved caspase-3 immunohistochemical staining.

2.10. Ki-67 and cleaved caspase-3 immunohistochemistry

For Ki-67 and cleaved caspase-3, heat-Induced epitope retrieval was performed by microwaving tissue sections in medium containing the antibody of interest, with10 mM citrate buffer at pH 6.0. Endogenous peroxidase was blocked with 3% hydrogen peroxide. Serum block was applied for 10 min with 10% normal horse serum. Sections were drained and incubated at room temperature with the primary antibody using conditions (Cleaved Caspase-3, Cell Signaling CS#9661, 1/600 overnight; Ki67, Novus, NB110-90592, 1/700, 1 h) as previously optimized. This was followed with a biotin labeled anti-rabbit secondary antibody (Vector Labs) for 30 min and horseradish peroxidase-conjugated ultrastreptavidin labeling reagent (ID Labs.) for 30 min. After washing well in TBS, color development was done with freshly prepared DAB (SK4105: Vector Labs). Slides were dehydrated and placed on coverslips. For Ki-67, the ‘percent positive nuclei’ was calculated by using commercial software (Nuclear v9, Aperio, Leica Biosystems) with default settings. Cleaved Caspase-3 (‘positive cells/ total cells’) and FOLR1 expression were also calculated (Positive Pixel Count v9 with default setting, Aperio).

2.11. FP biodistribution in orthotopic model

FPs or non-targeted porphysomes were injected intravenously when the tumor was at around 5 mm diameter detected by CT imaging. The animals were then euthanized at different time points. The fluorescence images at different post-injection time points in the A549

(FOLR+) orthotopic lung tumor model tumor were compared and 6 h post-injection of nanoparticles was chosen for imaging, because it showed the maximum fluorescence among all time points. The *in vivo* biodistribution of porphysome was assessed at the 6h post-injection. The animals were then euthanized and organs of interest were dissected: whole lung with tumors, heart, kidney, liver, spleen, small intestine, large intestine and hind limb muscle. The porphyrin accumulation in each organ was first detected by *ex vivo* fluorescence images using a wide-field imager (Maestro® EX 2.10, Cambridge Research & Instrumentation, Inc., Waltham, MA, USA) with 575-605 nm excitation and >645 nm detection using 500 ms integration time. For the biodistribution analysis, dissected tissues were freshly weighed and homogenized in 1 mL PBS. Triton X-100 was added to achieve 1%v/v final concentration. The suspension was centrifuged and the fluorescence of the supernatant was measured by spectrofluorimetry to calculate the amount of porphyrin. The percent injected dose per gram (%ID/g) was calculated for each organ based on a standard pyro-lipid concentration curve (N≥3). The porphysome accumulation in tumor and normal lung was further compared by fluorescent microscopy. Tissues were frozen in OCT gel using dry ice, sectioned (5 µm) and stained with DAPI. The frozen slides were imaged by confocal fluorescence microscopy using a 60X oil-immersion lens (633 nm excitation for porphyrin, 408 nm excitation for nuclei-staining DAPI). Orthotopic models using H460 and SBC5 cell lines (FOLR1+) were also prepared using the same inoculation procedure. When tumors were detected by CT scanning, 10 mg/kg of FP was injected IV. The mice were sacrificed 6 h later and lung containing tumor nodules was dissected and their fluorescence was imaged (Maestro®) with 575-605 nm excitation and >645 nm detection using 500 ms integration time.

2.12. Statistical Analysis

The student t-test (two-tailed) and one-way ANOVA was used to determine the statistical difference when comparing treatment groups. All statistical analyses were performed using StatView version 5.0 software (SAS Institute, Cary, NC, USA).

3. Results

3.1. Expression of FOLR1 in clinical lung cancer tissues and lung cancer cell lines

The expression of FOLR1 was significantly higher and occurred with higher frequency in metastatic lymph node samples from patients with advanced lung cancer taken by EBUS-TBNA and measured by qRT-PCR compared with normal lung and lymph node tissues (**Fig. 1A**). FOLR1 protein expression as determined by TMA analysis of resected lung cancer specimens was categorized FOLR1 according to the staining intensity and representative examples are shown in **Fig. 1B**. Positive staining of tumor cells generally showed a cytoplasmic and membrane pattern. Almost no staining was observed in normal lung tissue that also did not show the weak focal membrane staining of bronchiolo-alveolar cells that has reported previously (**Fig. 1C**) (27). Of the 333 lung cancer cases examined, 102 cases (30.6%) were FOLR1 positive, comprising 91 (42.1%) ADCs, 5 (5.7%) SqCCs and 3 (15.8%) LCCs (15.8%) (**Table 1**). No significant correlation was found between FOLR1 positivity and any clinicopathological parameters (data not shown).

Western blot analysis showed that FOLR1 is highly-expressed in the majority of lung cancer cell lines (**Fig. 1D**), so that A549, H647, H460 and SBC5 were selected as the FOLR1-positive cells and DFC1024 as a negative control.

3.2. FP uptake and PDT efficacy in vitro

The cellular uptake of FPs, measured by confocal fluorescence microscopy (20) showed that neither cells treated with saline as a negative control nor any cells incubated with non-targeted porphysomes for 3 h demonstrated detectable fluorescence signal (**Fig. 2A_i**). By contrast, FOLR1-positive A549, H647, H460 and SBC5 cells had strong intracellular florescence following 21 h incubation in medium containing FPs while the FOLR1-negative DFC1024 cells exhibited no fluorescence (**Fig. 2A_ii**). Specific FOLR1-mediated fluorescence activation of FPs was further validated by treating with free folic acid as an inhibitor prior to FP incubation and no fluorescence was seen in any of the cell lines (**Fig. 2A_iii)**), indicating that the free folic acid bound to folate receptor and so prevented FP binding. Hence, given that the fluorescence of porphysomes is fully quenched in the intact state, these *in vitro* experiments demonstrated the specificity of folate receptor-mediated cellular internalization of FPs and subsequent target-triggered porphyrin activation.

Fig. 2B shows the cell viability in the FOLR+ A549 and SBC5 cells following FP-PDT, with no treatment and PDT using non-targeted porphysomes as control. Non-targeted porphysome induced minor photocytotoxicity (86.2 and 82.8% viability at 5 and 10J/cm^2 light dose, respectively) in A549 but not in SBC5 cells (105.6 and 98.7%), while FP-PDT significantly decreased the cell viability in A549 (37.4 and 27.5%) and SBC5 (29.9 and 23.7%). In the dark controls (no laser light exposure), the cell viability remained high in A549 (105.9, 92.1 and 105.7%) and SBC5 cells (98.7, 104.9 and 100.8%) after incubation with non-targeted porphysomes, FPs and FPs plus free folic acid at a porphyrin concentration of 5×10^{-6}M.

3.3. FP uptake and PDT efficacy in the subcutaneous lung tumor model

Fluorescence activation serves as a direct indicator of porphysome uptake *in vivo*. The fluorescence of non-targeted porphysomes and FPs was first examined using a whole-body scanner in the subcutaneous H460 and A549 human (FOLR1+) tumor models and also served to determine the optimal PDT treatment time. There was significantly higher fluorescence in the tumor than the surrounding tissues at 6 h post IV injection (**Supplementary Fig. S1**).

The *in vivo* PDT efficacy was evaluated firstly by monitoring tumor growth in the A549 subcutaneous model. Since the tumors were easily accessible, direct laser light illumination was used for transdermal treatment (100 J/cm^2 at 100 mW/cm^2). The tumor fluorescence was first detected immediately prior to PDT treatment to ascertain the accumulation and fluorescence activation of FPs at 6 h post-injection (**Fig. 3A**). During treatment, a thermal camera was used to confirm minimal temperature increase due to the light exposure in both the laser-only controls (1.6 ± 0.52 °C) and the FP-PDT group (2.33 ± 0.42 °C) (**Fig. 3B**). No obvious tumor response was seen in the light-only controls and the tumors started to reach the end point on day 21 post-PDT (**Fig. 3C**). By contrast, with FRs-enabled PDT (FPs-PDT), the tumors first became swollen at 24-48 h post- PDT because of edema, then had dark brown scabs from day 3 to day 7 (**Fig. 3C**), which gradually resolved in the following 1-2 weeks. FP-PDT completely inhibited tumor growth for at least the 3 three weeks of observation, while the light-only controls continued to grow at the pre-treatment rate as the no-treatment group. Hence, FP-PDT showed significant therapeutic effect on tumor growth compared with the no-treatment (P <0.001) and laser-only (P <0.001) controls (**Fig. 3D)**.

We then examined the efficacy of PDT delivered by means of a 550 μm diffusing-type interstitial optical fiber (Biolitec biomedical technology GmbH, Jena, Germany) placed into the center tumor to simulate transbronchial application (**Figs. 4A_i, ii**). A549 subcutaneous xenografts of 9-10 mm in diameter (usually at 2-3 weeks after inoculation) were randomly separated into 5 treatment groups: no treatment, 100 or 200 J/cm^2 laser-only and FP-PDT at 100 or 200 J/cm^2. Light was delivered at 6 h after IV injection of FPs at a dose of 10 mg porphyrin /kg body weight. The animals were sacrificed 24h later and tumors were dissected and examined by H&E and immunohistochemical (Ki-67 and cleaved caspase-3) staining. The FPs-PDT group (both 100 and 200 J/cm^2) showed marked decrease in Ki-67 cell proliferation index and significant induction of apoptosis seen by cleaved caspase-3 positivity (**Figs. 4B and C**). There was no statistical difference between the 100 and 200 J/cm^2 treatments**.**

3.4. FP uptake in the orthotopic lung tumor model

As seen in **Fig 5A**, both FPs and non-targeted porphysomes accumulated more in the A549 tumor than in the lung and the fluorescence signal was higher in the former since cellular internalization further enhanced the fluorescence unquenching. Tumor nodules as small as 1 mm diameter could be detected (**Fig 5A_ii**). **Fig 5B** shows quantitative biodistribution measurements that were comparable (P <0.05) for FPs and non-targeted porphysomes in the lung (0.24 ± 0.11 % vs 0.31 ± 0.07% in injected dose per gm) and liver (0.43 ± 0.16% vs 0.38 ± 0.04%).

Using confocal microscopy, at 6 h post-injection fluorescence was clearly visible in the cytoplasm of the tumor cells, confirming intracellularization and unquencing of FPs (**Fig. 5C**).

The accumulation of folate-porphysomes in orthotopic tumor was further evaluated in FOLR1+ H460 and SBC5 (**Supplementary Fig. S2**).

4. Discussion

PDT is used to treat localized cancer as an alternative or adjunct to conventional therapies. Its high tumor selectivity results from the combination of tumor-preferential accumulation of photosensitizer and localized light irradiation. Although PDT has been successfully used for other indications, its use in lung cancer has been limited to centrally-located lesions either for treatment in carcinoma *in-situ* or for palliation in advanced obstructing lung cancer (9, 10). CT-guided percutaneous PDT for peripheral lesions is still investigational (30). Here, we aimed to explore image-guided PDT enabled by folate-porphysomes as activatable photosensitizers, in treating peripheral lung cancer and metastatic lymph nodes.

Folate receptor is an appropriate target to enhance photosensitizer uptake in lung cancers. Folate receptor 1 (FOLR1) is a glycoprotein that is anchored to the apical cell membrane of normal epithelial cells (31) and binds folate at high affinity to mediate transmembrane transport into the cytoplasm (32). FOLR1 is overexpressed in various cancers including NSCLC (31, 33-38). Its expression may vary by NSCLC histological subtype: for example, 74-87% of ADC and only 13-57% of SqCC were FOLR1-positive (27, 32). These treads were consistent with our TMA results, where FOLR1 was positively expressed in 42% of lung ADC with much lower expression in SqCC (5.7%) (**Table 1**). Although our staining rate seems to be lower than the previous studies, the more specific monoclonal FOLR1 antibody used here has been only become recently available, which may account for this difference.

qRT-PCR showed that 8 out of 17 cases (47%) were FOLR1-positive in metastatic lymph nodes using EBUS-TBNA samples. These findings were also consistent with a previous report where advanced tumors demonstrated similar levels of FOLR1 expression to surgically-resected tumors, by both the average expression scores and the frequency of any expression (32). Given the fact that FOLR1 expression is limited in normal lung or normal lymph node tissues based on our immunohistochemistry (**Fig. 1C**) and qRT-PCR results (**Fig. 1A**), FOLR1 should an excellent target for treating lung cancer by fluorescence image-guided tumor-targeted PDT (20), taking advantage of the unquenching, i.e. recovery of the constituent porphyrin fluorescence and photodynamic activity, upon FOLR1-mediated tumor cell uptake. The targeting efficiency and FOLR1-mediated activation of FPs were demonstrated in multiple FOLR1+ lung cancer cell lines *in vitro* (**Fig. 2**). The therapeutic efficacy was confirmed by both increased survival (**Fig. 3**) and histological analysis (**Fig. 4**).

In terms of clinical translation, it is worth noting that PDT can be performed repeatedly to ensure tumor destruction with minimal damage to the adjacent host tissue and critical normal structures (39). In addition, the porphyrin fluorescence could enable image-guide tumor dissection, through a combination of surgery and PDT for peripheral lung cancer. Previously, PDT with the first-generation photosensitizer Photofrin® has been evaluated in a phase II trial for NSCLC patients with pleural spread, where patients underwent either PDT only or surgery with complete resection or tumor debulking followed by intrapleural PDT (40). This trial established the feasibility of PDT to treat lung cancer in combination with surgery, but several toxicities were noted, including immediate postoperative death as a result of adult respiratory distress syndrome (ARDS) that was interpreted as PDT related. Compared to Photofrin, FP nanoparticles have the advantage of marked tumor-preferential accumulation after systematic

administration, as shown here in the orthotopic lung tumor models (26) (**Fig. 5A** and **Supplementary Fig. S2**), together with potent PDT efficacy that may improve the ability to achieve selective tumor ablation with minimal adverse effects.

Although we successfully demonstrated FP targeting in the orthotopic FOLR1+ peripheral lung cancer model, we could not conduct a survival study since because the laser fiber was too large to be inserted through the bronchus to perform PDT locally. For the future we plan to conduct survival studies using rabbits bearing orthotopically-transplanted tumors (13) and a pseudotumor model in pigs (ongoing trial, unpublished data), with bronchoscopic or EBUS-guidance to deliver the laser light to peripheral tumors, similarly to local photothermal therapy that we reported previously (41). Bronchoscopic or EBUS-guided FP-PDT should have the advantages of tumor-specific tissue destruction and minimal side effects, because of both tumor-preferential accumulation of the photosensitizer and localized laser irradiation. Placement of one or more optical fibers in the proper position(s) within the tumor mass will be required to achieve full-volume ablation, especially in the case of large tumors. Navigational bronchoscopy allows precise, minimally-invasive access to peripheral lung tumors and we have developed real-time tracking, navigation and fusion of endobronchial images using electromagnetic (EM) sensors in the endoscope tip (42, 43). Thereby, we can generate 3D virtual images of the airway based on information from cone-beam CT co-registered with real-time white-light and fluorescence bronchoscopic images (12). The latter will also yield information on the patient-specific tumor uptake of photodynamically-active FP porphyrin, that can be integrated into PDT treatment planning, as we have previously reported in multi-fiber PDT of whole prostate in patients (44) to enable optimal PDT treatment delivery in peripheral lung cancer.

Finally, porphysomes have a liposomal nanostructure allowing modification of the formulation to provide additional functions. Firstly, targeted porphysomes can be formulated using other ligands, such as VEGF and EGFR, to selectively target tumor cells based on the characterization of lung cancer type. Secondly, porphyrins are natural metal chelators, including radionuclides such as ^{64}Cu for PET imaging (45) or Mn^{3+} for MRI (46) for lung cancer detection, localization and staging. In addition, other pharmaceutical agents such as anti-angiogenic or chemotherapeutic drugs can be loaded into either the porphysome bilayer or core for combinational therapies (47). Therefore, folate-porphysomes can be further modified to achieve personalized treatments.

In conclusion, we have evaluated the target-specificity and efficacy of folate-porphysome-mediated PDT in lung cancer with overexpressed FOLR1. These initial findings demonstrate the FOLR1-mediated and -activated fluorescence imaging and image-guided PDT promise high therapeutic efficacy in treating lung cancer with minimal damage to surrounding tissues and motivate further preclinical development and validation to inform future clinical translation.

(4,983 /5,000 words)

Acknowledgements

This work is currently supported by the Canadian Cancer Society Research Institute through an Impact grant (2016-2021, *Ultra-minimally invasive multi-modal image-guided therapeutics of lung cancer*, PI: Dr. Kazuhiro Yasufuku). We thank Dr. Ming-Sound Tsao (Departments of Laboratory Medicine and Pathobiology, University of Toronto/University Health Network) for providing the lung cancer cell lines used in this study. The authors are also grateful to Mr.

Takatomo Funayama, (Morphotechnology Inc., Sapporo, Japan) for immunohistochemical studies, and Ms. Judy McConnell and Ms. Alexandria Grindlay (Toronto General Hospital) for sample collection and laboratory management.

Conflict of interest statement

The authors have no conflict of interest to declare.

References

1. Siegel R, Ma J, Zou Z, Jemal A. Cancer statistics, 2014. CA: a cancer journal for clinicians 2014;64(1):9-29. Epub 2014/01/09.

2. Aberle DR, Adams AM, Berg CD, Black WC, Clapp JD, Fagerstrom RM, et al. Reduced lung-cancer mortality with low-dose computed tomographic screening. The New England journal of medicine 2011;365(5):395-409. Epub 2011/07/01.

3. Statistics Canada. Leading Causes of Death in Canada. Ottawa: Statistics Canada 2012.

4. Rosen JE, Salazar MC, Wang Z, Yu JB, Decker RH, Kim AW, et al. Lobectomy versus stereotactic body radiotherapy in healthy patients with stage I lung cancer. The Journal of thoracic and cardiovascular surgery 2016;152(1):44-54 e9. Epub 2016/05/02.

5. Das M, Abdelmaksoud MH, Loo BW, Jr., Kothary N. Alternatives to surgery for early stage non-small cell lung cancer-ready for prime time? Current treatment options in oncology 2010;11(1-2):24-35. Epub 2010/06/26.

6. Ikeda N, Usuda J, Kato H, Ishizumi T, Ichinose S, Otani K, et al. New aspects of photodynamic therapy for central type early stage lung cancer. Lasers in surgery and medicine 2011;43(7):749-54. Epub 2011/11/08.

7. Allison R, Moghissi K, Downie G, Dixon K. Photodynamic therapy (PDT) for lung cancer. Photodiagnosis and photodynamic therapy 2011;8(3):231-9. Epub 2011/08/26.

8. Shafirstein G, Battoo A, Harris K, Baumann H, Gollnick SO, Lindenmann J, et al. Photodynamic Therapy of Non-Small Cell Lung Cancer. Narrative Review and Future Directions. Annals of the American Thoracic Society 2016;13(2):265-75. Epub 2015/12/10.

9. Sandell JL, Zhu TC. A review of in-vivo optical properties of human tissues and its impact on PDT. Journal of biophotonics 2011;4(11-12):773-87. Epub 2011/12/15.

10. Simone CB, 2nd, Friedberg JS, Glatstein E, Stevenson JP, Sterman DH, Hahn SM, et al. Photodynamic therapy for the treatment of non-small cell lung cancer. Journal of thoracic disease 2012;4(1):63-75. Epub 2012/02/02.

11. Miyazu Y, Miyazawa T, Kurimoto N, Iwamoto Y, Kanoh K, Kohno N. Endobronchial ultrasonography in the assessment of centrally located early-stage lung cancer before photodynamic therapy. American journal of respiratory and critical care medicine 2002;165(6):832-7. Epub 2002/03/19.

12. Anayama T, Qiu J, Chan H, Nakajima T, Weersink R, Daly M, et al. Localization of pulmonary nodules using navigation bronchoscope and a near-infrared fluorescence thoracoscope. The Annals of thoracic surgery 2015;99(1):224-30. Epub 2014/12/03.

13. Anayama T, Nakajima T, Dunne M, Zheng J, Allen C, Driscoll B, et al. A novel minimally invasive technique to create a rabbit VX2 lung tumor model for nano-sized image contrast and interventional studies. PloS one 2013;8(6):e67355. Epub 2013/07/11.

14. Chen J, Stefflova K, Niedre MJ, Wilson BC, Chance B, Glickson JD, et al. Protease-triggered photosensitizing beacon based on singlet oxygen quenching and activation. Journal of the American Chemical Society 2004;126(37):11450-1. Epub 2004/09/16.

15. Zheng G, Chen J, Stefflova K, Jarvi M, Li H, Wilson BC. Photodynamic molecular beacon as an activatable photosensitizer based on protease-controlled singlet oxygen quenching and activation. Proceedings of the National Academy of Sciences of the United States of America 2007;104(21):8989-94. Epub 2007/05/16.

16. McDonnell SO, Hall MJ, Allen LT, Byrne A, Gallagher WM, O'Shea DF. Supramolecular photonic therapeutic agents. Journal of the American Chemical Society 2005;127(47):16360-1. Epub 2005/11/25.

17. Yogo T, Urano Y, Mizushima A, Sunahara H, Inoue T, Hirose K, et al. Selective photoinactivation of protein function through environment-sensitive switching of singlet oxygen generation by photosensitizer. Proceedings of the National Academy of Sciences of the United States of America 2008;105(1):28-32. Epub 2008/01/04.

18. Lovell JF, Jin CS, Huynh E, Jin H, Kim C, Rubinstein JL, et al. Porphysome nanovesicles generated by porphyrin bilayers for use as multimodal biophotonic contrast agents. Nature materials 2011;10(4):324-32. Epub 2011/03/23.

19. Jin CS, Zheng G. Liposomal nanostructures for photosensitizer delivery. Lasers in surgery and medicine 2011;43(7):734-48. Epub 2011/11/08.

20. Jin CS, Cui L, Wang F, Chen J, Zheng G. Targeting-triggered porphysome nanostructure disruption for activatable photodynamic therapy. Advanced healthcare materials 2014;3(8):1240-9. Epub 2014/01/28.

21. Kato T, Daigo Y, Aragaki M, Ishikawa K, Sato M, Kaji M. Overexpression of CDC20 predicts poor prognosis in primary non-small cell lung cancer patients. J Surg Oncol 2012. Epub 2012/04/11.

22. Kato T, Daigo Y, Aragaki M, Ishikawa K, Sato M, Kaji M. Overexpression of KIAA0101 predicts poor prognosis in primary lung cancer patients. Lung Cancer 2012;75(1):110-8. Epub 2011/06/22.

23. Kato T, Daigo Y, Aragaki M, Ishikawa K, Sato M, Kondo S, et al. Overexpression of MAD2 predicts clinical outcome in primary lung cancer patients. Lung Cancer 2011;74(1):124-31. Epub 2011/03/08.

24. Travis WD, Brambilla E, Burke AP, Marx A, Nicholson AG. WHO Classification of Tumours of the Lung, Pleura, Thymus and Heart. Fourth edition 2015.

25. Union for International Cancer Control (UICC), TNM Classification of Malignant Tumours. 7th ed. : Wiley-Blackwell; 2009.

26. Nakajima T, Anayama T, Matsuda Y, Hwang DM, McVeigh PZ, Wilson BC, et al. Orthotopic lung cancer murine model by nonoperative transbronchial approach. The Annals of thoracic surgery 2014;97(5):1771-5. Epub 2014/05/06.

27. O'Shannessy DJ, Yu G, Smale R, Fu YS, Singhal S, Thiel RP, et al. Folate receptor alpha expression in lung cancer: diagnostic and prognostic significance. Oncotarget 2012;3(4):414-25. Epub 2012/05/02.

28. Vrouenraets MB, Visser GW, Snow GB, van Dongen GA. Basic principles, applications in oncology and improved selectivity of photodynamic therapy. Anticancer research 2003;23(1B):505-22. Epub 2003/04/12.

29. Dolmans DE, Fukumura D, Jain RK. Photodynamic therapy for cancer. Nature reviews Cancer 2003;3(5):380-7. Epub 2003/05/02.

30. Okunaka T, Kato H, Tsutsui H, Ishizumi T, Ichinose S, Kuroiwa Y. Photodynamic therapy for peripheral lung cancer. Lung Cancer 2004;43(1):77-82. Epub 2003/12/31.

31. Weitman SD, Weinberg AG, Coney LR, Zurawski VR, Jennings DS, Kamen BA. Cellular localization of the folate receptor: potential role in drug toxicity and folate homeostasis. Cancer research 1992;52(23):6708-11. Epub 1992/12/01.

32. Nunez MI, Behrens C, Woods DM, Lin H, Suraokar M, Kadara H, et al. High expression of folate receptor alpha in lung cancer correlates with adenocarcinoma histology and EGFR [corrected] mutation. Journal of thoracic oncology : official publication of the International Association for the Study of Lung Cancer 2012;7(5):833-40. Epub 2012/06/26.

33. Chancy CD, Kekuda R, Huang W, Prasad PD, Kuhnel JM, Sirotnak FM, et al. Expression and differential polarization of the reduced-folate transporter-1 and the folate receptor alpha in mammalian retinal pigment epithelium. The Journal of biological chemistry 2000;275(27):20676-84. Epub 2000/04/29.

34. Toffoli G, Cernigoi C, Russo A, Gallo A, Bagnoli M, Boiocchi M. Overexpression of folate binding protein in ovarian cancers. International journal of cancer Journal international du cancer 1997;74(2):193-8. Epub 1997/04/22.

35. Ross JF, Chaudhuri PK, Ratnam M. Differential regulation of folate receptor isoforms in normal and malignant tissues in vivo and in established cell lines. Physiologic and clinical implications. Cancer 1994;73(9):2432-43. Epub 1994/05/01.

36. Bueno R, Appasani K, Mercer H, Lester S, Sugarbaker D. The alpha folate receptor is highly activated in malignant pleural mesothelioma. The Journal of thoracic and cardiovascular surgery 2001;121(2):225-33. Epub 2001/02/15.

37. Evans CO, Young AN, Brown MR, Brat DJ, Parks JS, Neish AS, et al. Novel patterns of gene expression in pituitary adenomas identified by complementary deoxyribonucleic acid microarrays and quantitative reverse transcription-polymerase chain reaction. The Journal of clinical endocrinology and metabolism 2001;86(7):3097-107. Epub 2001/07/10.

38. Weitman SD, Frazier KM, Kamen BA. The folate receptor in central nervous system malignancies of childhood. Journal of neuro-oncology 1994;21(2):107-12. Epub 1994/01/01.

39. Agostinis P, Berg K, Cengel KA, Foster TH, Girotti AW, Gollnick SO, et al. Photodynamic therapy of cancer: an update. CA: a cancer journal for clinicians 2011;61(4):250-81.

40. Friedberg JS, Mick R, Stevenson JP, Zhu T, Busch TM, Shin D, et al. Phase II trial of pleural photodynamic therapy and surgery for patients with non-small-cell lung cancer with pleural spread. Journal of clinical oncology : official journal of the American Society of Clinical Oncology 2004;22(11):2192-201. Epub 2004/06/01.

41. Jin CS, Wada H, Anayama T, McVeigh PZ, Hu HP, Hirohashi K, et al. An Integrated Nanotechnology-Enabled Transbronchial Image-Guided Intervention Strategy for Peripheral Lung Cancer. Cancer research 2016;76(19):5870-80. Epub 2016/08/21.

42. Weersink RA, Qiu J, Hope AJ, Daly MJ, Cho BC, Dacosta RS, et al. Improving superficial target delineation in radiation therapy with endoscopic tracking and registration. Medical physics 2011;38(12):6458-68. Epub 2011/12/14.

43. Qiu J, Hope AJ, Cho BC, Sharpe MB, Dickie CI, DaCosta RS, et al. Displaying 3D radiation dose on endoscopic video for therapeutic assessment and surgical guidance. Physics in medicine and biology 2012;57(20):6601-14. Epub 2012/09/27.

44. Trachtenberg J, Bogaards A, Weersink RA, Haider MA, Evans A, McCluskey SA, et al. Vascular targeted photodynamic therapy with palladium-bacteriopheophorbide photosensitizer for recurrent prostate cancer following definitive radiation therapy: assessment of safety and treatment response. The Journal of urology 2007;178(5):1974-9; discussion 9.

45. Liu TW, MacDonald TD, Shi J, Wilson BC, Zheng G. Intrinsically copper-64-labeled organic nanoparticles as radiotracers. Angewandte Chemie 2012;51(52):13128-31.

46. MacDonald TD, Liu TW, Zheng G. An MRI-sensitive, non-photobleachable porphysome photothermal agent. Angewandte Chemie International Edition 2014;53(27):6956-9. Epub 2014/05/21.

47. Sengupta S, Eavarone D, Capila I, Zhao G, Watson N, Kiziltepe T, et al. Temporal targeting of tumour cells and neovasculature with a nanoscale delivery system. Nature 2005;436(7050):568-72.

Table 1. Immunopositivity of folate receptor 1 (FOLR1) protein in lung cancers (n=333)

Histology	FOLR1-negative	FOLR1-positive	FOLR1 positive rate (%)
Adenocarcinoma (ADC)	125	91	42.1
Squamous Cell Carcinoma (SqCC)	82	5	5.7
Large Cell Carcinoma (LCC)	16	3	15.8
Adeno-Squamous Carcinoma (ASC)	2	1	33.3
Small Cell Lung Cancer (SCLC)	4	0	0.0
Mucoepidermoid Carcinoma	0	2	100.0
Carcinosarcoma	1	0	0.0
Atypical Carcinoid	1	0	0.0
Total	231	102	30.6 %

Figure Legends

Figure 1. Folate Receptor 1 (FOLR1) expression in lung cancer.

(**A**) qRT-PCR in metastatic lymph node samples from advanced lung cancer. Eight out of 17 cases (47%) are FOLR1-positive. The relative expression levels were normalized to the ACTB level in each sample and calculated as the threshold cycle (CT) value divided by the average CT values in normal lung. Error bar represents the standard error of the mean (SEM) of triplicates. ADC, adenocarcinoma; SqCC, squamous cell carcinoma; LCNEC, large-cell neuroendocrine carcinoma; Small, small-cell lung cancer; Negative, non malignant lymph nodes. (**B**) Representative examples of FOLR1 staining in lung adenocarcinomas by TMA analyses. (**C**) Minimal staining in normal lung tissue except for slight membrane staining on the alveolar cell surface. (**D**) Western blotting of lung cancer cell lines for FOLR1 expression. KB cells (oral carcinoma) with high FOLR1 expression were used as positive controls.

Figure 2. Cellular uptake and fluorescence activation and *in vitro* photocytotoxicity of folate-porphysomes (FPs) in FOLR1-positive lung cancer cells.

(**A**) The confocal fluorescence imaging of the selected lung cancer cells, including FOLR1-positive expression (H460, A549, SBC-5 and H647) and FOLR1-negative cell line DFC1024. (**i**) Fluorescence activation was not seen in the non-targeting porphysome treatment group. (**ii**) Fluorescence was detected in the cells treated by folate-porphysome in FOLR1-positive lung cancer cells. (**iii**) The internalization and fluorescence activation was inhibited at the presence of free folic acid. Images were taken 21 h post 3 h treatment incubation. Scale bar = 100 μm. (**B**) The targeting-triggered PDT activation of folate-porphysome was investigated by measuring the cell viability assay with and without laser treatment. PDT treatment method: 671 nm laser at 5 and 10 J/cm^2. Results are shows as mean ± SEM (bars) of 4 individual wells. Cell viability was normalized to that of the untreated cells.

Figure 3. *In vivo* PDT treatment response in A549 subcutaneous tumor-bearing mice.

Mice were injected with folate-porphysomes at a dose of 10 mg/kg. (**A**) Maestro fluorescence imaging of tumor at 6 h post-injection of folate-porphysomes; (**B**), Quantitative temperature increase during the PDT treatment, comparing the laser control group and folate-porphysome PDT group with n=3; (**C**), Representative mice tumor images at day 0, day 2, day 7, and day 14 post PDT treatment. After tumor has grown to 5-6mm in diameter, mice were injected with folate-porphysome or saline. The tumor was then irradiated with a 671 nm PDT fiber at 100 J/cm^2. (**D**) Tumor growth curve after treatment for each group. Significant decrease in the tumor size on 21 days after PDT treatment were seen for folate-porphysome-treated group.

Figure 4. *In vivo* therapeutic effect of FOLR1 targeting-triggered PDT using a diffusing-type laser.

(**A**) Schematic image of treatment; **i)** mice were inoculated with subcutaneous A549 tumor; **ii)** mice were IV injected with folate-porphysomes; **iii)** PDT was

conducted at 6 h post-injection using a cylindrical laser fiber inserting through the centre of the tumor. (**B**), Representative histopathological and immunohistochemical images of PDT treated tumors. Red spot = laser insertion point. Scale bar = 5 mm (**C**), Folate-porphysome mediated PDT treatment group showed much less Ki-67 staining the nuclei of proliferating cells positivity and much higher apoptotic effect to the entire tumor by cleaved caspase-3 staining compared to control groups.

Figure 5. *In vivo* fluorescence activation and biodistribution in nude mice with A549 orthotopic lung cancer model.

(**A**) Representative fluorescence images of tumors withe heart and lungs 6 h post-injection of **i)** non-targeting porphysome and **ii)** folate-porphysome with a dose of 10 mg/kg porphyrin content. (**B**) Accumulation of folate-porphysome and non-targeting porphysome in organs harvested 6 h after administration in mice. Y-axis label shows % injected dose/gram (%ID/g). (**C**) Histology analysis including **i)** H&E and **ii)** confocal microscopy images of A549 cells showing both porphyrin fluorescence activation of the cytoplasmic distributions.

Figure 1

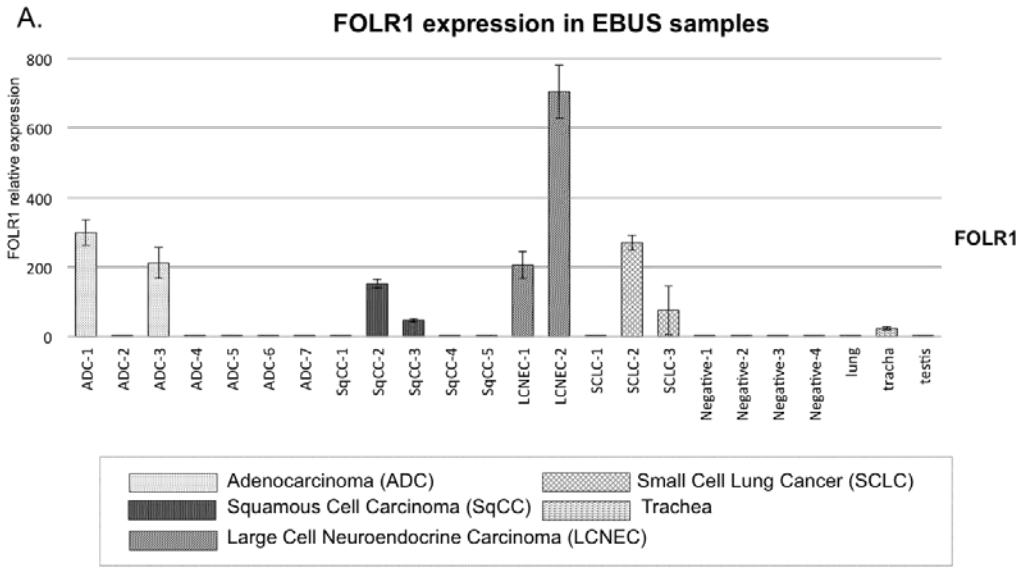
A.
FOLR1 expression in EBUS samples
FOLR1 relative expression
800
600
400
200
0
ADC-1
ADC-2
ADC-3
ADC-4
ADC-5
ADC-6
ADC-7
SqCC-1
SqCC-2
SqCC-3
SqCC-4
SqCC-5
LCNEC-1
LCNEC-2
SCLC-1
SCLC-2
SCLC-3
Negative-1
Negative-2
Negative-3
Negative-4
lung
tracha
testis
Adenocarcinoma (ADC)
Squamous Cell Carcinoma (SqCC)
Large Cell Neuroendocrine Carcinoma (LCNEC)
Small Cell Lung Cancer (SCLC)
Trachea

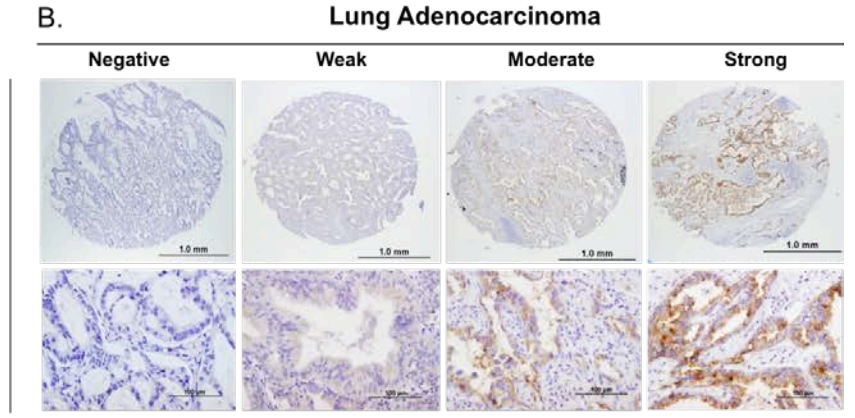
B.
Lung Adenocarcinoma
Negative
Weak
Moderate
Strong
FOLR1

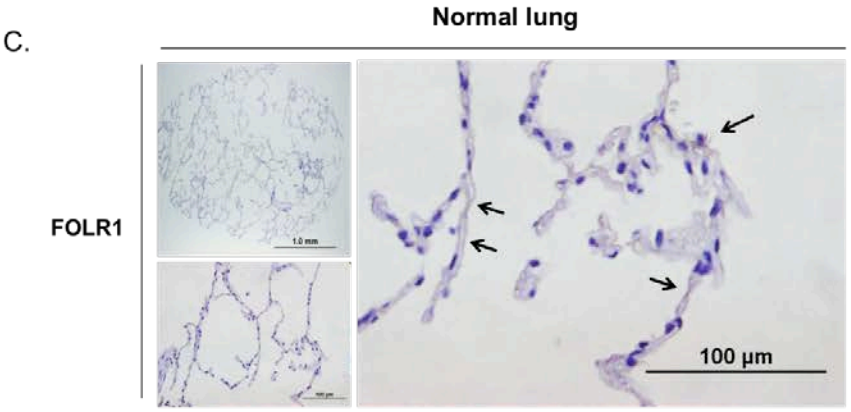
C.
Normal lung
FOLR1
100 µm

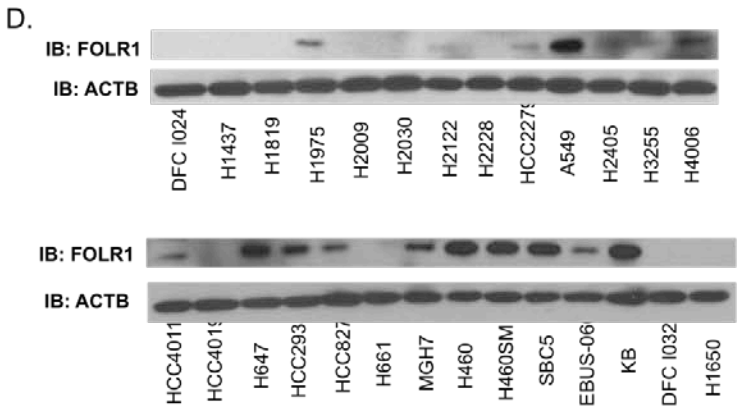
D.
IB: FOLR1
IB: ACTB
DFC I024
H1437
H1819
H1975
H2009
H2030
H2122
H2228
A549
H2405
H3255
H4006
IB: FOLR1
IB: ACTB
H647
H661
MGH7
H460
SBC5
KB
DFC I032
H1650

Figure 2A

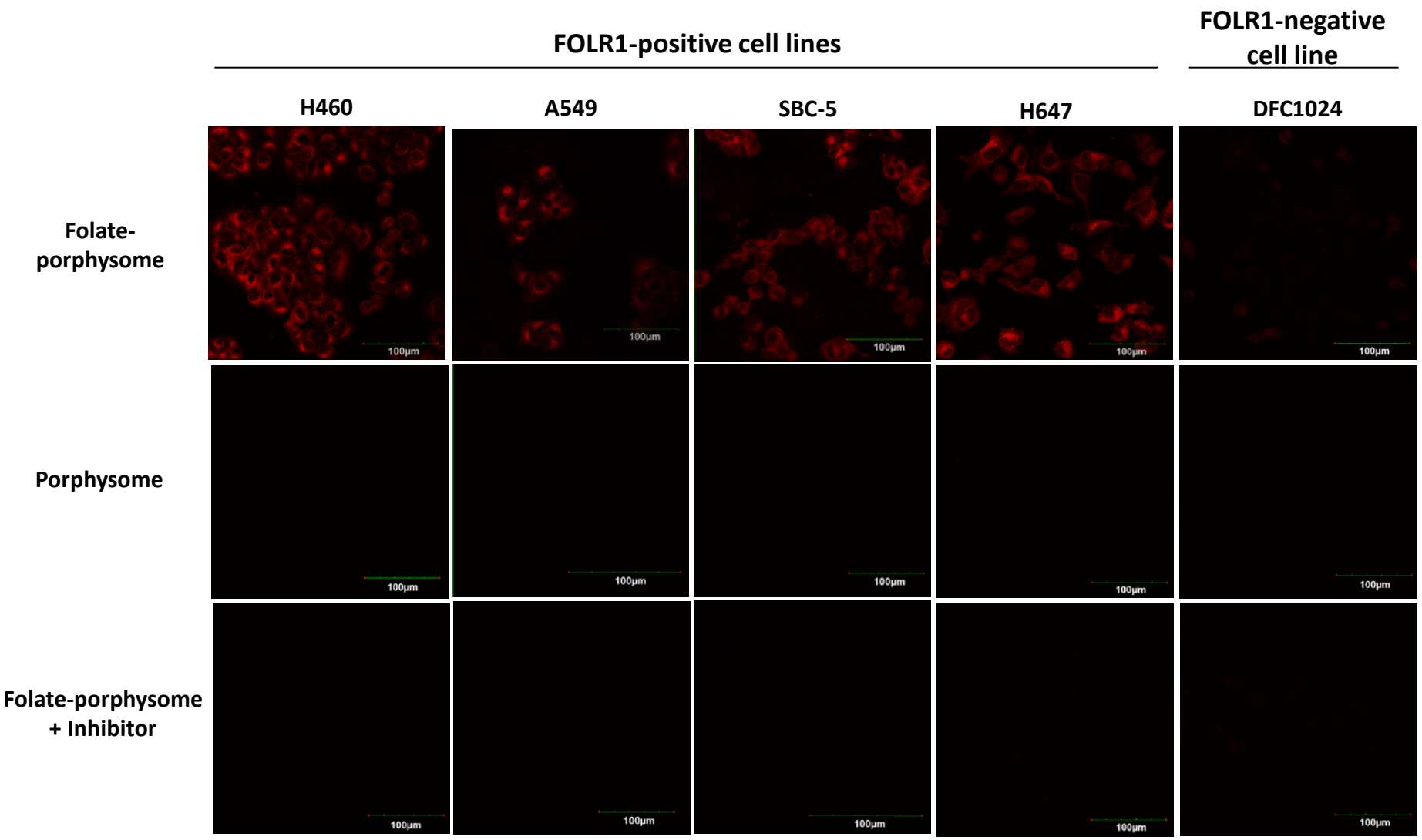
FOLR1-positive cell lines
FOLR1-negative cell line
H460
A549
SBC-5
H647
DFC1024
Folate-porphysome
Porphysome
Folate-porphysome + Inhibitor
100μm

Figure 2B

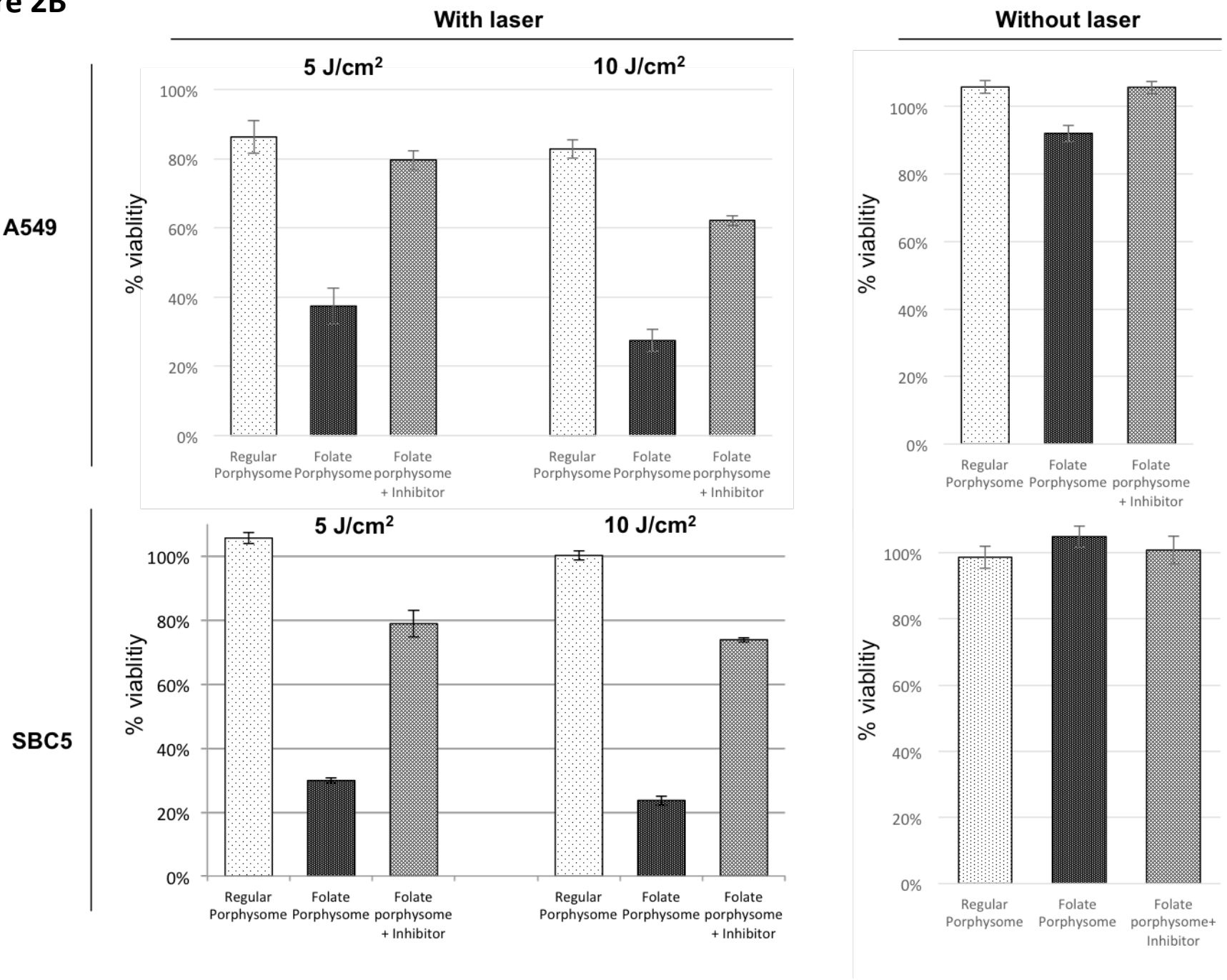
With laser
Without laser
A549
SBC5
5 J/cm²
10 J/cm²
% viablitiy
100%
80%
60%
40%
20%
0%
Regular Porphysome
Folate Porphysome
Folate porphysome + Inhibitor
Folate porphysome+ Inhibitor

Figure 3

A. Fluorescence imaging

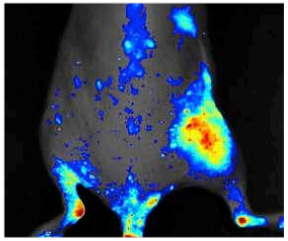

B. Temperature change

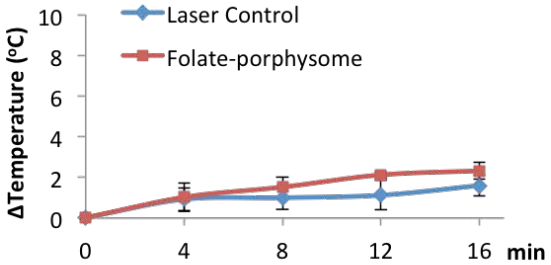

C. Survival study

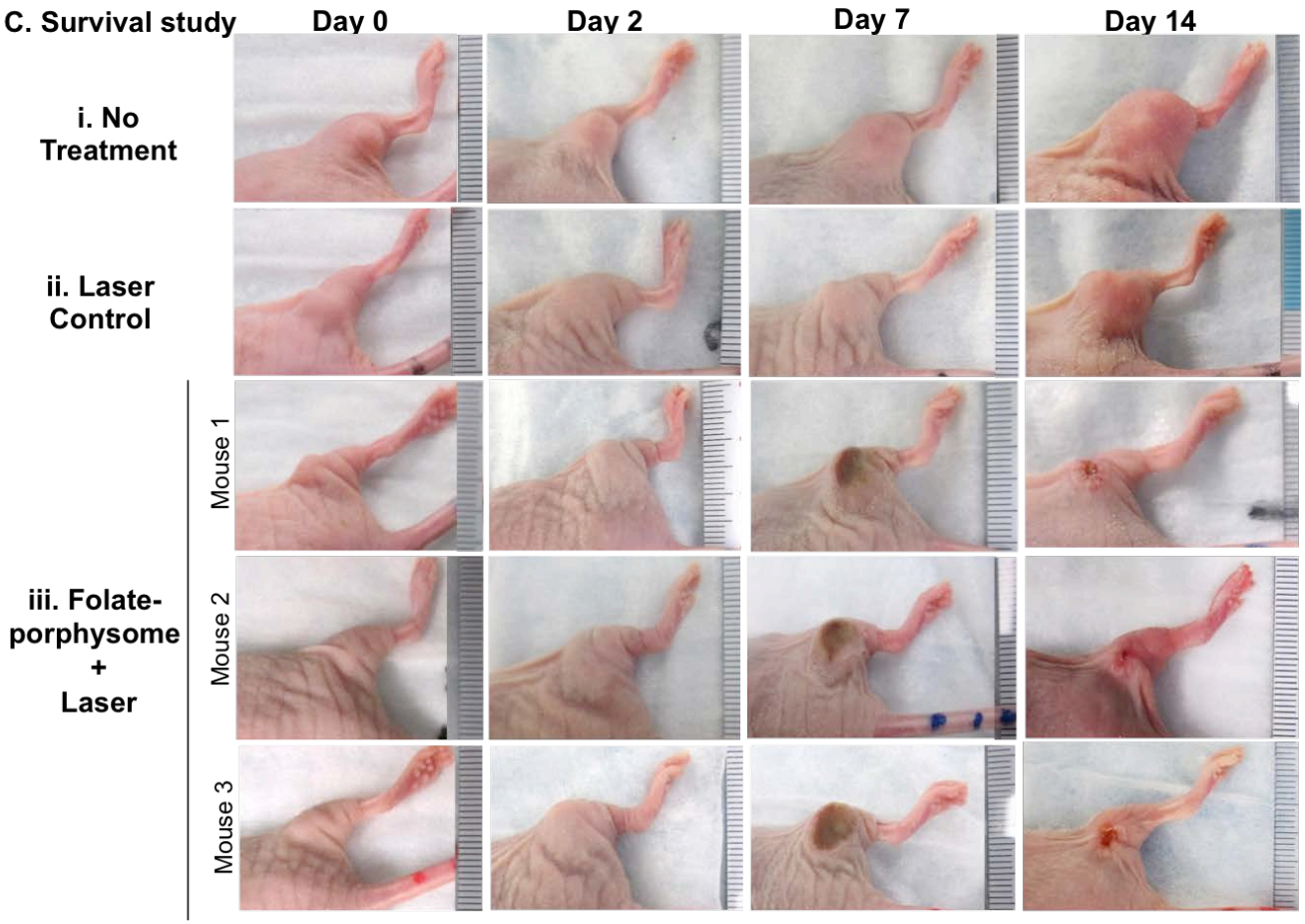

D. Post-treatment tumor growth curve

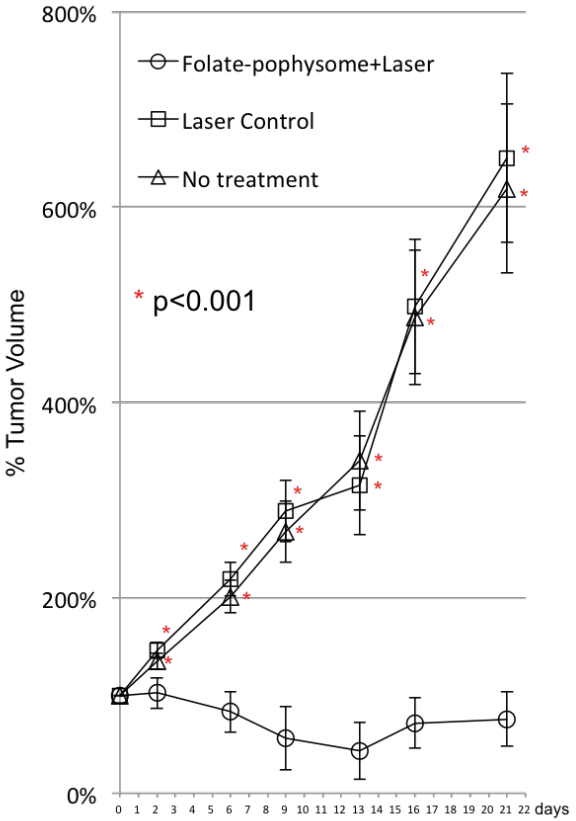

Figure 4

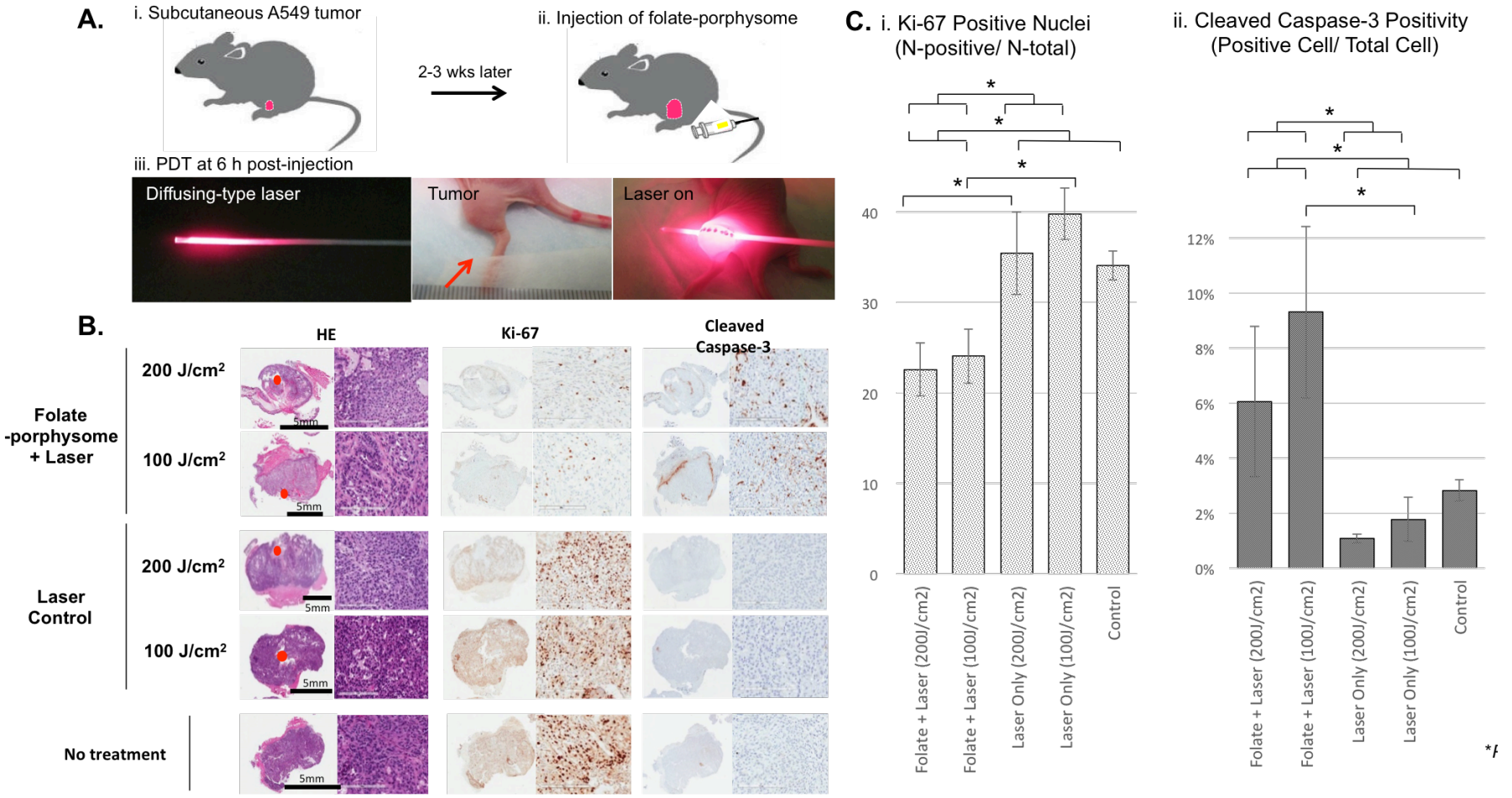
A.
i. Subcutaneous A549 tumor
2-3 wks later
ii. Injection of folate-porphysome
iii. PDT at 6 h post-injection
Diffusing-type laser
Tumor
Laser on
B.
HE
Ki-67
Cleaved Caspase-3
Folate -porphysome + Laser
200 J/cm²
100 J/cm²
Laser Control
200 J/cm²
100 J/cm²
No treatment
5mm
C. i. Ki-67 Positive Nuclei (N-positive/ N-total)
0
10
20
30
40
Folate + Laser (200J/cm2)
Folate + Laser (100J/cm2)
Laser Only (200J/cm2)
Laser Only (100J/cm2)
Control
ii. Cleaved Caspase-3 Positivity (Positive Cell/ Total Cell)
0%
2%
4%
6%
8%
10%
12%
Folate + Laser (200J/cm2)
Folate + Laser (100J/cm2)
Laser Only (200J/cm2)
Laser Only (100J/cm2)
Control

Figure 5

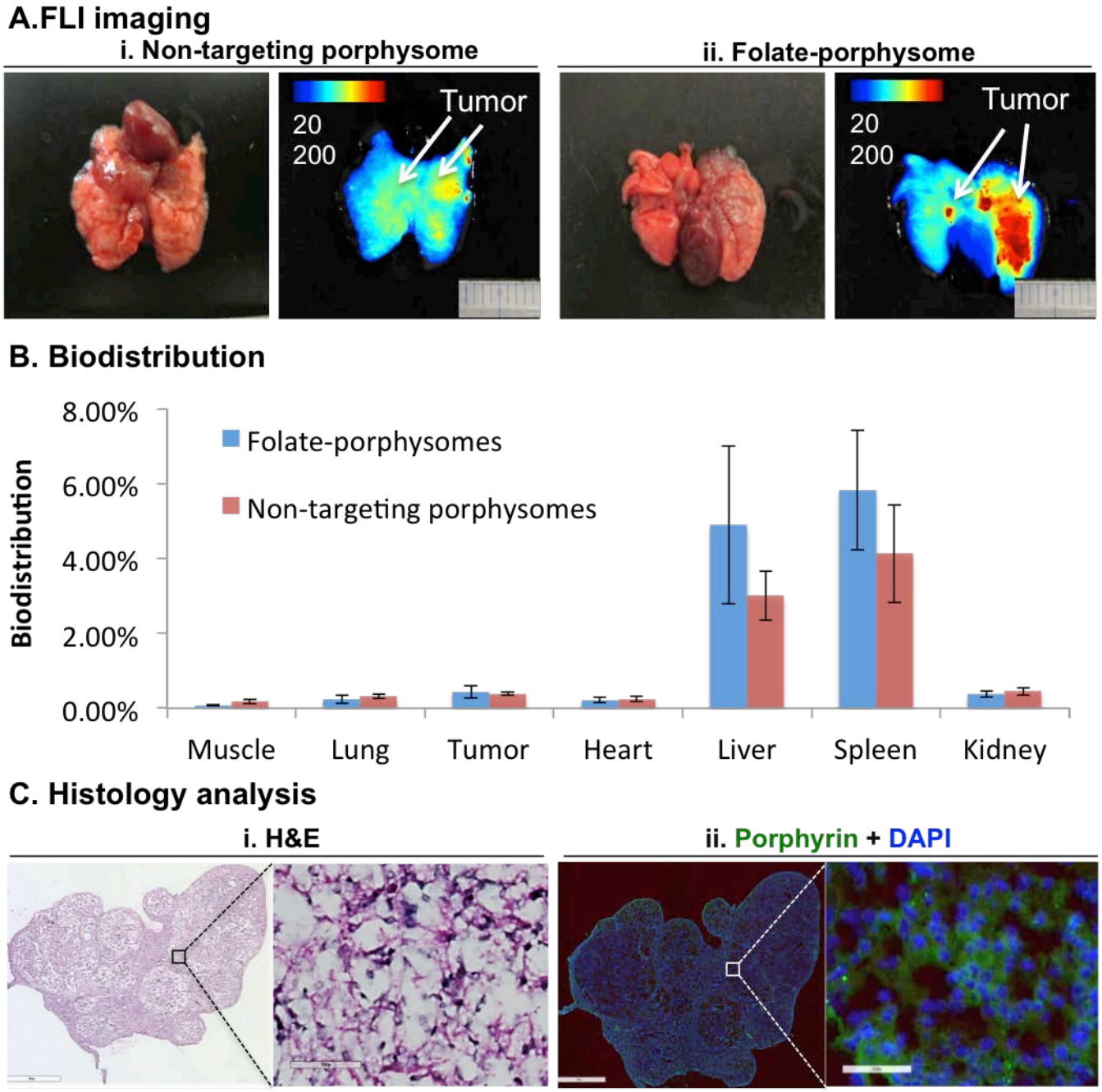
A.FLI imaging
i. Non-targeting porphysome
ii. Folate-porphysome
Tumor
20
200
Tumor
20
200
B. Biodistribution
Biodistribution
8.00%
6.00%
4.00%
2.00%
0.00%
Folate-porphysomes
Non-targeting porphysomes
Muscle
Lung
Tumor
Heart
Liver
Spleen
Kidney
C. Histology analysis
i. H&E
ii. Porphyrin + DAPI